Mode-specificity of vibrationally coherent internal conversion in rhodopsin during the primary visual event

Christoph Schnedermann, Matz Liebel, and Philipp Kukura*

Physical and Theoretical Chemistry Laboratory, South Parks Road, Oxford OX1 3QZ, UK

E-mail: philipp.kukura@chem.ox.ac.uk

Abstract

Conical intersections play a crucial role in photochemical processes but limited experimental information exists on the structural distortions that couple electronic with reactive nuclear motion. Using ultra-broadband and highly time-resolved optical spectroscopy, we follow the evolution of vibrational wavepackets after passage through a conical intersection during the primary visual event, the 11-*cis* to all-*trans* photoisomerisation of the retinal chromophore in rhodopsin. Comparison of nuclear coherences generated with resonant to off-resonant impulsive excitation conclusively reveals coherent wavepacket motion in the bathorhodopsin photoproduct over the full vibrational manifold. We observe strongly enhanced coherences in low-frequency torsional degrees of freedom over the fingerprint region and almost complete suppression of some hydrogen wagging motion. Our ability to monitor the multi-dimensional evolution of nuclear wavepackets across multiple electronic states is a general means for studying the structural and dynamic origins of efficient photochemistry and provides critical experimental information for theoretical studies.

*To whom correspondence should be addressed

Introduction

Photoisomerisation reactions are ideally suited to study the origins of fast and efficient photochemistry.[1–6] Absorption of a photon causes electronic excitation and provides molecules with excess energy, which is converted into atomic motion to drive the reaction.[7–11] A classic example is the 11-*cis* to all-*trans* photoisomerisation of the retinal chromophore in rhodopsin marking the first step in vision.[12–14] Recently, ultrafast transient absorption spectroscopy provided evidence for the involvement of a conical intersection (CI) in this reaction,[15] also demonstrated in biomimetic photoswitches.[16] Theoretical studies have proposed backbone torsion, pyramidalisation and hydrogen wagging to be crucially involved in the mechanism, but there is little experimental information on the identity of the nuclear degrees of freedom that contribute to the formation of the CI.[13,14,17–20]

To illustrate the dynamic evolution of a system in a photochemical reaction mediated by a CI, it is instructive to consider a simplified potential energy diagram (Fig. 1). Following population of the first excited electronic state, the system quickly evolves out of the Franck-Condon (FC) region towards the CI. Here, internal conversion to the ground state surface takes place, leading to the formation of photoproduct and back reversion to the reactant.[21] The kinetics of such photoreactions are often studied by time-resolved pump-probe spectroscopy.[1,15,21,22] A short resonant pump pulse photoexcites the molecule and is followed by a probe pulse, which records a transient absorption spectrum at various time-delays after the pump pulse. By using an ultra-short pump pulse ($\sim$10 fs), the excitation process additionally generates coherent vibrational wavepackets in all FC-active modes.[23] The resulting wavepacket motion modulates the transient absorption signal, thus providing vibrational information in addition to the electronic dynamics.[23,24] Such wavepacket motion can be highly affected by passage through a CI depending on the involvement of the underlying degree of freedom in the CI,[25,26] implying that monitoring vibrational coherence after internal conversion could provide detailed information on the structure of the CI.

We have recently demonstrated that internal conversion through a CI is vibrationally

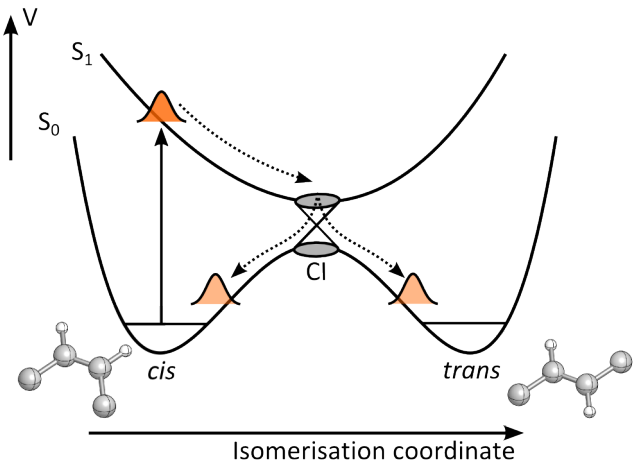

Figure 1: Schematic potential energy diagram for a *cis* to *trans* photoisomerisation mediated by a conical intersection (CI). Excited molecules rapidly leave the Franck-Condon region towards the CI mediating internal conversion to the ground state potential. The overall reaction leads to the formation of photoproduct (*trans*) and back reversion to the reactant (*cis*).

coherent.[23] In the case of the $S_2 \leftarrow S_1$ transition in β-carotene, we observed strong similarities between the spectrum from coherences passing through the CI and the Raman spectrum of the S1 product state, with some weak bands in the fingerprint region enhanced upon internal conversion. In the case of rhodopsin, such an experimental approach uncovered a dominant low-frequency torsional coherence after internal conversion assigned to the primary photoproduct bathorhodopsin.[22] The employed pump pulses, however, remained too long and the spectroscopic sensitivity too low to reveal the fate of higher frequency modes suggested by theory to be significant contributors to the photoisomerisation. A detailed understanding of the CI region and the factors connecting chemical reactivity and efficiency on an atomic level is therefore still missing.

Results and Discussion

We performed transient absorption spectroscopy of rhodopsin with an unprecedented combination of time-resolution ($\sim$10 fs), ultrabroad detection bandwidth (500 - 900 nm) and spectroscopic sensitivity ($\sim$10 μOD). In particular the high spectroscopic sensitivity is a

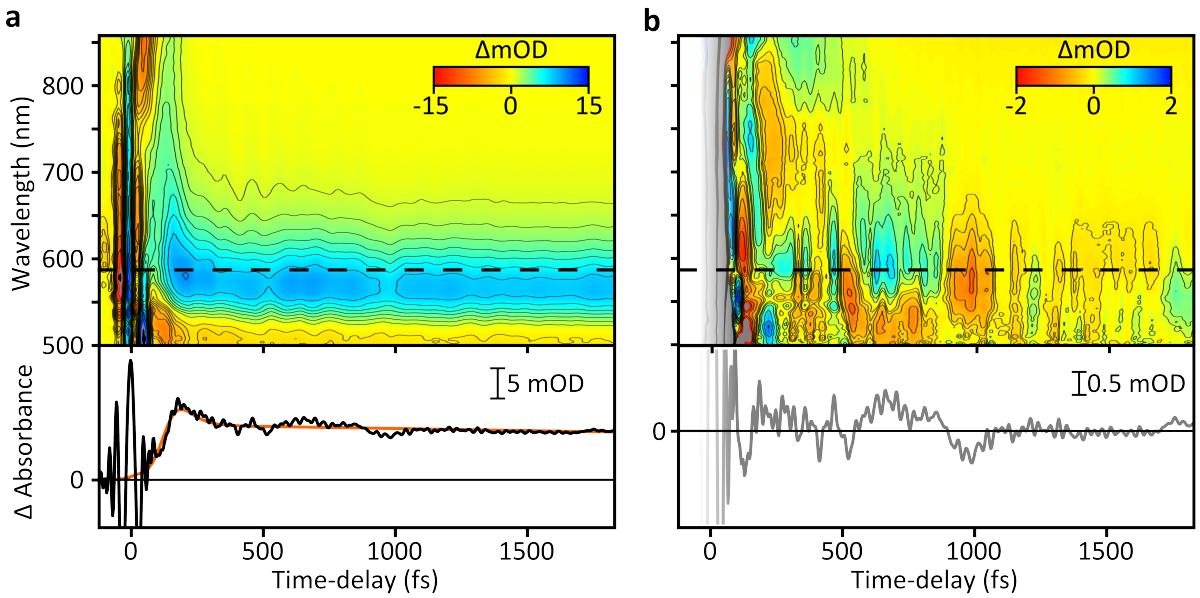

Figure 2: Transient electronic and vibrational signatures after photoexcitation of rhodopsin with a 8 fs pulse. (a) Differential absorbance exhibiting a coherent artifact at early time-delays and the appearance of photoproduct absorption at 560 nm. The transient at 587 nm illustrates the growth of the photoinduced absorption within 200 fs and is shown together with the corresponding fit to the electronic kinetics (orange). (b) After subtraction of the electronic response by global fitting, the underlying vibrational coherences become visible as illustrated by the transient at 587 nm. Early time-points dominated by the coherent artifact have been shaded for clarity as they are not included in further analysis.

critical advance over previous studies and allows us to reveal nuclear coherences over the full vibrational manifold that cause small oscillatory features on top of the transient absorption spectra. The corresponding differential absorbance map after photoexcitation with an 8 fs pulse centered at 500 nm is shown in Fig. 2a. Around zero time-delay, we observe a coherent artifact followed by a rapidly red shifting stimulated emission band initially appearing at 800 nm. After leaving the probe window in the near-IR, the stimulated emission converts into a photoinduced absorption signal, which blue shifts to its final maximum at 560 nm indicating formation of bathorhodopsin within 200 fs.[15,22] Longer time-delays (>200 fs) exhibit a stationary transient absorption spectrum with overlapping signatures of ground state bleach (498 nm) and bathorhodopsin absorption (560 nm). Individual transients such as that shown at 587 nm furthermore reveal large oscillatory modulations of the electronic signal caused by the generation of vibrational wavepackets upon photoexcitation.

We are able to extract the residual vibrational coherence as a function of the probe wavelength (Fig. 2b) by globally fitting the electronic dynamics of the transient absorbance map, as indicated for the transient in Fig. 2a. The coherent oscillations are most pronounced in the 500 - 650 nm window with a node near the bathorhodopsin absorption maximum at 560 nm.[24] The oscillations contain both high- and low-frequency components lasting for more than 1.5 ps, as indicated by the transient at 587 nm. Probe wavelengths >700 nm, however, exhibited only very short-lived coherence activity. Wavelength-dependent Fourier transformation of the residual coherences reveals the spectral intensity distributions of all vibrational modes up to 1700 cm^{-1} (Fig. 3a). We find pronounced activity in the torsional (<500 cm^{-1}), hydrogen-out-of-plane (HOOP, 800 - 1100 cm^{-1}), C-C stretching (1150 - 1350 cm^{-1}) and the C=C stretching (1500 - 1650 cm^{-1}) regions. Additionally, the overall wavelength-dependence of the Fourier intensities closely resembles the absorption spectra of rhodopsin and bathorhodopsin with maxima at 500 nm and 580 nm, respectively.

To rationalize the molecular origin of the vibrational coherences in the bathorhodopsin absorption window, we compare an averaged Fourier power spectrum (570 - 640 nm) with the resonance Raman (RR) spectrum of bathorhodopsin (Fig. 3b). We chose the 570 - 640 nm window specifically due to the known dependence of the coherent amplitudes on the shape of the underlying absorption spectrum (see Fig. 3a).[29] In the high-frequency region (>1000 cm^{-1}) we find signatures of bathorhodopsin C-C stretching modes at 1208 cm^{-1}, 1237 cm^{-1} and 1267 cm^{-1} with matching relative intensity distributions, as well as a shoulder at 1535 cm^{-1} assigned to the C=C stretching mode in bathorhodopsin, albeit with decreased relative intensity. The low-frequency torsional region shows enhanced activity compared to the RR spectrum, with a pronounced mode at 60 cm^{-1}, previously shown to originate from coherently excited bathorhodopsin.[22] The HOOP region is dominated by an intense band at 865 cm^{-1}, which we attribute to the unresolved C_{10}-H and C_{12}-H HOOPs at 850 cm^{-1} and 875 cm^{-1}, respectively. We furthermore note the distinct lack of coherent activity in the C_{11}-H HOOP at 920 cm^{-1}.

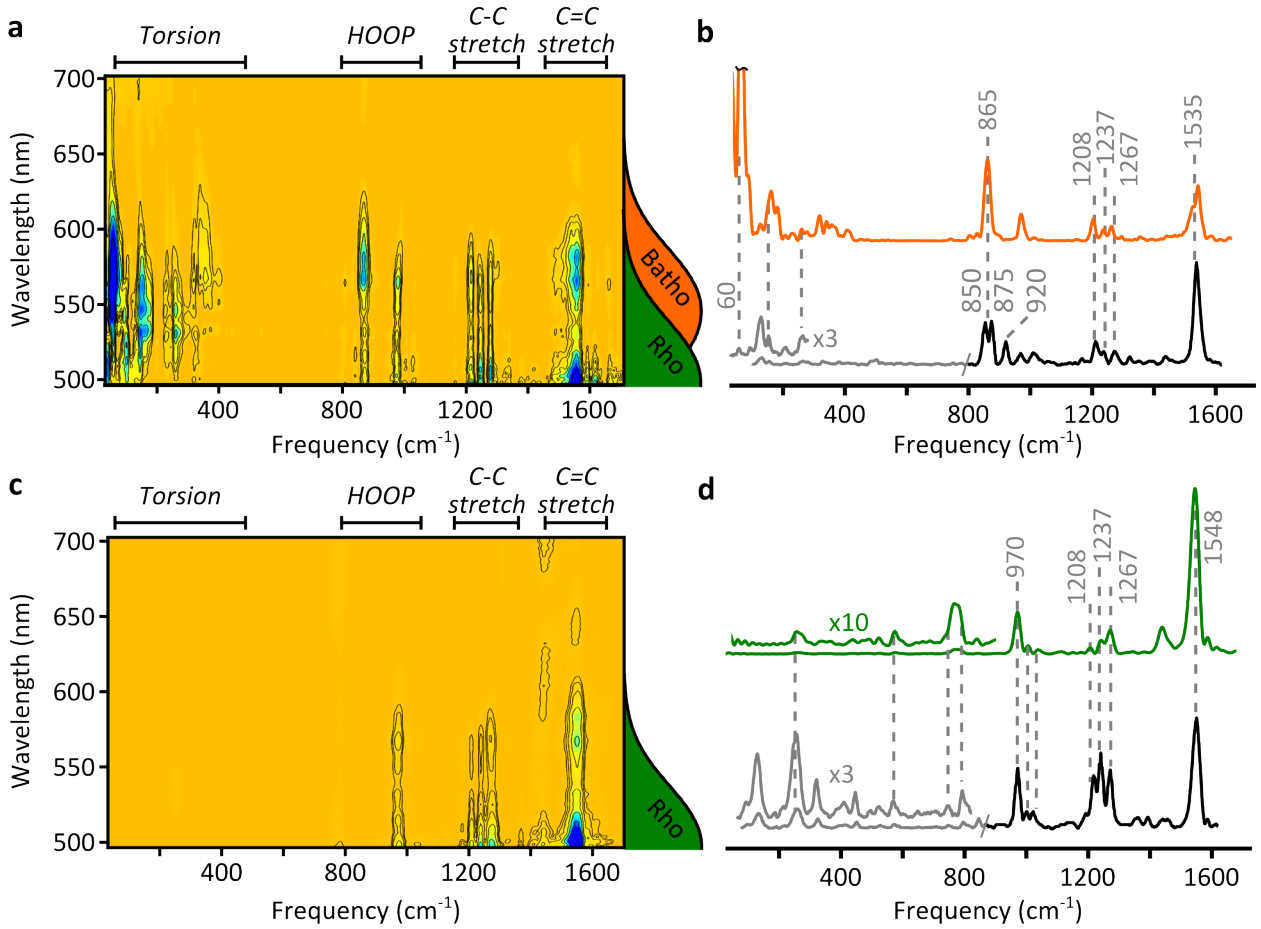

Figure 3: Fourier transform power maps and spectra compared to resonance Raman. (a) Fourier power map following resonant excitation with an 8 fs pump pulse centered at 500 nm and (b) resonance Raman spectrum (grey, black) compared to a spectral average from 570 - 640 nm for bathorhodopsin (orange). (c) Fourier power map following off-resonant excitation with a 9 fs pulse centered at 800 nm and (d) resonance Raman spectrum (grey, black) compared to a spectral average from 570 - 640 nm for rhodopsin (green). The pump-probe data has been scaled to correct for amplitude effects caused by finite time-resolutions (see supporting information Fig. S3). Resonance Raman spectra are adapted with permission from Lin et al[27] (488 nm, grey), copyright (1998) American Chemical Society and Kukura et al[28] (805 nm, black), copyright (2005) American Association for the Advancement of Science. We remark in this context, that the RR spectrum of rhodopsin and bathorhodopsin is largely invariant to a change in the excitation wavelength (see supporting information Fig. S4). Absorption spectra for rhodopsin (orange) and bathorhodopsin (green) are indicated on the side of (a) and (c), respectively. Time-domain power spectra were obtained by Fourier transformation of the residual coherence map for time delays greater than 80 fs.

Resonant excitation by an ultra-short pump pulse generates coherent wavepacket motion on both ground and excited states,[30] complicating the interpretation of the vibrational co-

herences. It is thus necessary to record a pure ground state time-domain spectrum which can be achieved in an off-resonant pump-probe experiment. Keeping the probe pulse unchanged and using a 9 fs pump pulse centred at 800 nm, we completely avoid photoexcitation and only generate wavepacket motion on the ground state of rhodopsin.[31,32] The resulting Fourier power map (Fig. 3c) exhibits coherent activity in the HOOP, C-C stretch and C=C stretch regions but lacks all intensity in the torsional region of the spectrum. The overall wavelength-dependence of the coherent activity is shifted towards the shorter wavelength region compared to the on-resonant experiment, now closely resembling the absorption spectrum of rhodopsin. The Fourier power spectrum averaged over the same probe window (570 - 640 nm) as for the on-resonant experiment exhibits a HOOP band at 970 cm^{-1}, three C-C stretches at 1208 cm^{-1}, 1237 cm^{-1} and 1267 cm^{-1} and an intense C=C stretch at 1548 cm^{-1}, in excellent agreement with the ground state RR spectra of rhodopsin.[27,28]

The coherence activity obtained in the off-resonant experiment is related to the RR intensities, as shown by the similarity to the RR spectrum of rhodopsin in Fig. 3d. Resonant probing thereby ensures proportionality to the RR cross-sections, yielding comparable intensities to a RR spectrum.[29] The use of an ultra-short on-resonant pump pulse, however, will generate wavepackets in all FC-active modes on the excited electronic state. After preparation, these wavepackets will rapidly evolve out of the FC region and through the CI before they arrive on the photoproduct potential energy surface. For a fully coherent reaction, a resonantly probed photoproduct spectrum would equal the corresponding RR spectrum, for the same reasons as in the off-resonant case.

This allows us to assign, which modes in Fig. 3a, b correspond to bathorhodopsin and which to rhodopsin coherences. In the low-frequency region, no coherent activity can be detected in the off-resonant experiment (Fig. 3c), while resonant excitation leads to very strong coherent activity centered around the absorption maximum of bathorhodpsin. These bands must hence originate from (vibrationally hot) bathorhodopsin, such as the intense band at 865 cm^{-1}, which does not appear in the off-resonant experiment and is

a clear marker band of bathorhodopsin.[27,28] Its wavelength-dependent coherent activity is also centered around the absorption maximum of bathorhodopsin. We furthermore attribute the appearing shoulder at 1535 cm^{-1} to the C=C stretch of the photoproduct, since the off-resonant experiment does not show such a characteristic signature. The C-C stretch region is difficult to assign due to the mutual Raman signatures of reactant and product (compare Fig. 3b, d). However, resonant excitation significantly shifts the wavelength-dependent coherence activities towards the bathorhodopsin absorption spectrum, while the reactant shows most activity near the absorption maximum of rhodopsin. The spectral average displayed in Fig 3b additionally ranks the intensities in order of: 1208 cm^{-1} > 1237 cm^{-1} > 1267 cm^{-1}, while the opposite is found in Fig 3d, suggesting that, despite overlap, we observe vibrational coherences in ground state bathorhodopsin modes. We therefore assign all bands in the resonant spectrum to bathorhodopsin with the exception of the bands at 970 cm^{-1} and 1548 cm^{-1}.

CIs are, however, theoretically predicted to affect wavepacket propagation significantly depending on the type of involvement in the formation of the CI.[25,26] Passage through a CI should therefore lead to a change of the coherent vibrational activity in a pump-probe experiment. In the case of rhodopsin, differences between the coherence activity after internal conversion and the RR spectrum of bathorhodopsin therefore provide information on the CI geometry. Theoretical studies have categorised the vibrational degrees of freedom involved in the formation of a CI into tuning and coupling modes.[25,26] Tuning modes are required to reach the CI energetically by reducing the energy gap between the involved electronic states, whereas coupling modes are active in forming the CI. Based on this description, wavepackets in tuning modes are expected to be largely unaffected by the internal conversion event while coupling mode wavepackets will be strongly influenced.

Comparison of the RR and coherence spectra of bathorhodopsin allows us to divide the Raman-active modes into three categories: those that are strongly enhanced (< 500 cm^{-1}), those that exhibit expected relative intensities (500 - 1600 cm^{-1}) and those that are unexpect-

edly weak (920 cm^{-1}). Fig. 4a illustrates the dynamic evolution of vibrational wavepackets in a coupling mode in the vicinity of a CI.[25,26] Photoexcitation of a molecular ensemble by an ultra-short pump pulse generates wavepackets on the excited electronic state, which initially evolve in-phase. Upon encountering the CI, a fraction of the excited molecules internally converts,[33] leading to wavepackets oscillating on the photoproduct potential. The wavepackets in the remaining molecules on the excited electronic state revisit the CI half a vibrational period later, again forming photoproduct wavepackets after internal conversion. The successively arriving photoproduct wavepackets are therefore necessarily out-of-phase with each other, provided the vibrational period is shorter than the excited state lifetime. The signal recored in an ensemble measurement will hence be diminished due to destructive interference. Coherence activity in coupling modes can be further reduced in intensity due to their high anharmonic character near the CI which leads to a delocalisation of the vibrational wavepacket, as pointed out by Kühl et al.[25] We remark, however, that an alternative explanations based on a phase-dependent conical intersection space may be equally valid.[34] Which model is ultimately responsible for the lack of coherence activity in the C_{11}-H mode, however, will require further detailed quantum chemical calculations guided by the experimental results reported here.

Vibrational wavepackets in tuning modes on the other hand are not strongly affected by such a phase relationship (Fig. 4b).[25,26] In rhodopsin, the isomerisation is volume-conserving and spatially localised. The involved reactant and photoproduct potentials are therefore not significantly displaced giving rise to coherence activities comparable to the RR spectrum. Minor deviations from the expected RR intensities in such modes can, however, be rationalised by considering a small change in the potential energy surface upon internal conversion. If the photoisomerisation proceeds with a change of frequency or displacement along a tuning mode, then internal conversion will project wavepackets on a slightly steeper or shallower part of the photoproduct surface. This results in a small perturbation in the wavepacket dynamics causing minor intensity deviations compared to the RR spectrum due to partially

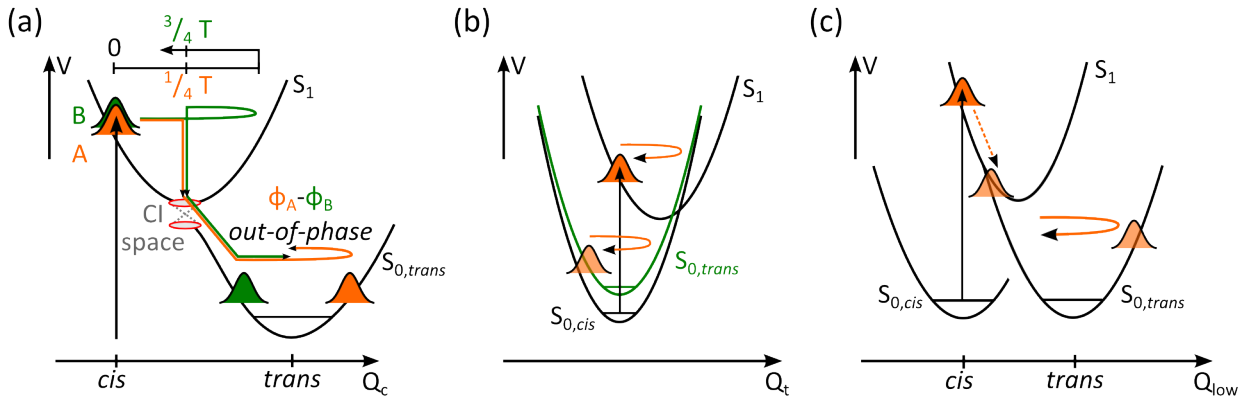

Figure 4: Schematic representation of wavepacket dynamics. (a) Coupling modes: Upon encountering the CI a fraction of the excited molecules internally convert forming wavepackets on the photoproduct *trans* potential energy surface (A, orange). Remaining excited state wavepackets (B, green) cross to the *trans* surface half a vibrational period (T) later resulting in out-of-phase wavepacket motion and hence destructive interference due to accumulated phase difference $\phi_A - \phi_B$. The coherent activity is drastically decreased compared to a RR spectrum. We remark, that the CI space contains a multitude of CIs with different geometries, one of which has been chosen to represent the behaviour of wavepackets in coupling modes. (b) Tuning modes: Vibrational wavepackets created in the excited state will reduce the energy gap between the involved electronic states leading to internal conversion. However, these modes are not part of the CI space and are thus unaffected by the crossing. Wavepackets will, after change of the electronic state, simply continue to oscillate in the new potential. Since reactant and photoproduct potentials are minimally displaced in rhodopsin, this leads to coherence activities similar to RR. (c) Low-frequency modes: Large initial displacements on the excited state lead to high accumulated momentum on the excited state which is subsequently transferred to the photoproduct potential giving rise to large coherent activity observed in the photoproduct. Note that Q_{low} refers to photoproduct normal coordinates rather than the reaction coordinate itself, which is a complex combination of the above.

destructive interference. These effects are particularly small for the photoisomerisation in rhodopsin, since the volume-conserving nature of the reaction leaves most modes unchanged as apparent by the overall similarity of C-C and C=C stretching region in the RR spectra of rhodopsin and bathorhodopsin.[15]

Finally, the low-frequency region of the time-domain spectrum is characterised by a number of very intense bands including the previously reported bathorhodopsin band at 60 cm^{-1}. Theoretical simulations[13,17] and RR intensity analysis[35] show, that low-frequency modes are experiencing a steep slope on the excited potential energy surface, leading to

fast relaxation particularly along these coordinates. However, for vibrational modes such as the backbone torsion at 60 cm^{-1}, corresponding to a 555 fs vibrational period, the short excited state lifetime (50 - 100 fs) necessarily implies only minimal structural evolution along that coordinate on the excited state. Since the overall isomerisation reaction requires a large localised torsional rearrangement, the rapid internal conversion projects wavepackets in these modes on a very steep part of the photoproduct potential energy surface. This leads to enhanced nuclear motion and results in pronounced coherent activity (Fig. 4c). This, on the other hand, does not exclude significant twisting along the C_{11}=C_{12} dihedral coordinate, as predicted by quantum chemical studies,[13,17] as this reaction coordinate represents a linear combination of many normal modes, including modes with much higher frequencies and thus shorter vibrational periods.

Based on this theoretical description and extensive previous theoretical efforts,[7,13,14,17] we assign the coherent activity observed in the C-C streching region (1208 cm^{-1}, 1237 cm^{-1}, 1267 cm^{-1}), the $C_{10/12}$-H HOOP bands (850 cm^{-1}, 875 cm^{-1}) and the C=C stretching shoulder at 1535 cm^{-1} to tuning modes of the isomerisation reaction. This assignment is further supported by the excited state lifetime of rhodopsin (70 - 100 fs) requiring high-frequency FC-active modes with short vibrational periods to act as efficient tuning coordinates. Minor deviations from the RR intensities as seen for the $C_{10/12}$-H HOOP or the C=C stretch are likely due to different frequencies in ground and excited states.[25] The complete lack of activity in the 920 cm^{-1} mode in the on-resonant time-domain spectrum (Fig. 3b) suggests that the C_{11}-H HOOP is one of the major coupling modes of the system. This assignment is also supported by recent high-level quantum mechanical calculations suggesting an asynchronous bicycle-pedal motion with major involvement of the C_{11}-H HOOP.[13] We remark that our technique is surprisingly insensitive to the photo- to bathorhodopsin structural relaxation previously observed with femtosecond stimulated Raman spectroscopy[28] (see supplementary information), resulting in a Fourier power spectrum that mainly reflects the properties of the final (hot) bathorhodopsin photoproduct.

Conclusions

We have used ultrafast transient absorption spectroscopy with high temporal resolution and spectroscopic sensitivity to investigate the fate of nuclear wavepackets generated by photoexcitation after internal conversion mediated by a CI during a photochemical process. When comparing the coherence spectrum after passage through the CI with the RR spectrum of the photochemical product, we observed both strong enhancement and suppression of coherences. This behavior is in contrast to that observed during the S_2-S_1 internal conversion in β-carotene.[23] There, some high-frequency (>600 cm^{-1}) coherences are amplified while the other band intensities remain unchanged. The major difference between the two systems is that in β-carotene only small structural changes are coupled to the internal conversion, while a complete photoisomerisation is driven in rhodopsin. As a result, we observe clear differences in coherence intensities compared to the RR spectrum of bathorhodopsin that can be explained by the displacement of the respective potential energy surfaces upon internal conversion. On the one hand, our results provide a strong proving ground for theoretical studies, especially in the comparison of how nuclear wavepackets are affected by a CI for reactive and unreactive processes. On the other hand, the ability to monitor vibrational coherences throughout chemical reactions and across multiple electronic surfaces is likely to provide detailed insight into the mechanistic and structural origins of ultrafast processes such as charge and proton transfer, singlet fission and photochemical transformations in general.

Experimental

Sample preparation

Rhodopsin (OD_{500} = 15) was obtained from the rod outer segments of bovine retinae and purified by sucrose flotation followed by sucrose density gradient centrifugation, as described by Grip et al.[15,36] Hydroxylamine was added to a final concentration of 2 mM to suppress

the accumulation of photoproduct.

Ultrafast spectroscopy.

A Pharos-6W amplifier system provided 180 fs pulses at 1030 nm (1.05 W, 1 kHz). 2 mW of the output generated white light (WL) in a 3 mm Sapphire crystal and was used as the probe pulse after removal of the fundamental. The second harmonic (515 nm) pumped a one-stage noncollinear optical parametric amplifier (NOPA) to generate off-resonant pump pulses centered at 800 nm. A two-stage NOPA pumped by the second harmonic provided a narrowband output at 780 nm which was used to generate WL in a 3 mm Sapphire crystal. This WL acted as a seed in a 1-stage NOPA pumped by the third harmonic (343 nm) of the laser system to produce resonant excitation pulses centered at 500 nm. Pulses were compressed to sub-10 fs duration by a combination of chirped mirrors and a pair of fused silica wedges (Layertec). The pulse durations were confirmed by second-harmonic-generation frequency resolved optical gating (SHG-FROG) employing a 10 μm BBO crystal.[37]

Transient absorption traces were recorded using a pump chopping scheme and the transmitted probe was sent onto a home-built single-shot prism spectrograph using a CMOS-array detector for broadband detection. The samples were flowed through a 200 μm path length flowcell (120 μm windows) by a peristaltic pump at a rate to ensure replenishment of the sample between consecutive pulses. Pump and probe diameters in the focus were 75 and 50 μm^2 with corresponding pulse energies set to 60 nJ (resonant pump), 120 nJ (off-resonant pump) and 2 nJ (WL probe), respectively.

Acknowledgement

The EPSRC supports P.K. through a Career Acceleration Fellowship (EP/H003541/1). We thank Giovanni Bassolino and Katelyn Spillane for purification of the rhodopsin sample.

Supporting Information Available

Pulses and data processing as well as simulations on previously observed frequency shifts in the HOOP region. This material is available free of charge via the Internet at `http://pubs.acs.org/`.

References

(1) Takeuchi, S.; Ruhman, S.; Tsuneda, T.; Chiba, M.; Taketsugu, T.; Tahara, T. *Science* **2008**, *322*, 1073–7.

(2) Dobryakov, A. L.; Ioffe, I.; Granovsky, A. A.; Ernsting, N. P.; Kovalenko, S. A. *J. Chem. Phys.* **2012**, *137*, 244505.

(3) Wand, A.; Gdor, I.; Zhu, J.; Sheves, M.; Ruhman, S. *Annu. Rev. Phys. Chem.* **2013**, 437–58.

(4) Kraack, J. P.; Buckup, T.; Motzkus, M. *J. Phys. Chem. Lett.* **2013**, 383–7.

(5) Bismuth, O.; Friedman, N.; Sheves, M.; Ruhman, S. *Chem. Phys.* **2007**, *341*, 267–75.

(6) Domcke, W.; Yarkony, D. R. *Annu. Rev. Phys. Chem.* **2012**, *63*, 325–52.

(7) Hahn, S.; Stock, G. *J. Phys. Chem. B* **2000**, *104*, 1146–9.

(8) Lasorne, B.; Worth, G. A.; Robb, M. A. *Wiley Interdiscip. Rev. Comput. Mol. Sci.* **2011**, *1*, 460–75.

(9) Rostov, I. V.; Amos, R. D.; Kobayashi, R.; Scalmani, G.; Frisch, M. J. *J. Phys. Chem. B* **2010**, *114*, 5547–55.

(10) Virshup, A. M.; Punwong, C.; Pogorelov, T. V.; Lindquist, B. A.; Ko, C.; Martínez, T. J. *J. Phys. Chem. B* **2009**, *113*, 3280–91.

(11) Léonard, J.; Schapiro, I.; Briand, J.; Fusi, S.; Paccani, R. R.; Olivucci, M.; Haacke, S. *Chem. Eur. J.* **2012**, *18*, 15296–304.

(12) Wald, G. *Science* **1968**, *162*, 230–9.

(13) Schapiro, I.; Ryazantsev, M. N.; Frutos, L. M.; Ferré, N.; Lindh, R.; Olivucci, M. *J. Am. Chem. Soc.* **2011**, *133*, 3354–64.

(14) Weingart, O.; Garavelli, M. *J. Chem. Phys.* **2012**, *137*, 22A523.

(15) Polli, D.; Altoè, P.; Weingart, O.; Spillane, K. M.; Manzoni, C.; Brida, D.; Tomasello, G.; Orlandi, G.; Kukura, P.; Mathies, R. a.; Garavelli, M.; Cerullo, G. *Nature* **2010**, *467*, 440–3.

(16) Briand, J.; Bräm, O.; Réhault, J.; Léonard, J.; Cannizzo, A.; Chergui, M.; Zanirato, V.; Olivucci, M.; Helbing, J.; Haacke, S. *Phys. Chem. Chem. Phys.* **2010**, *12*, 3178–87.

(17) Frutos, L. M.; Andruniów, T.; Santoro, F.; Ferré, N.; Olivucci, M. *Proc. Natl. Acad. Sci. USA* **2007**, *104*, 7764–9.

(18) Schapiro, I.; Weingart, O.; Buss, V. *J. Am. Chem. Soc.* **2009**, *131*, 16–7.

(19) Strambi, A.; Coto, P. B.; Frutos, L. M.; Ferré, N.; Olivucci, M. *J. Am. Chem. Soc.* **2008**, *130*, 3382–8.

(20) Weingart, O. *Chem. Phys.* **2008**, *349*, 348–55.

(21) Mathies, R.; Brito Cruz, C.; Pollard, W. T.; Shank, C. V. *Science* **1988**, *240*, 777–9.

(22) Wang, Q.; Schoenlein, R.; Peteanu, L. A.; Mathies, R.; Shank, C. V. *Science* **1994**, *266*, 422–4.

(23) Liebel, M.; Schnedermann, C.; Kukura, P. *Phys. Rev. Lett.* **2014**, *112*, 198302.

(24) Liebel, M.; Kukura, P. *J. Phys. Chem. Lett.* **2013**, *4*, 1358–64.

(25) Kühl, A.; Domcke, W. *J. Chem. Phys.* **2002**, *116*, 263–74.

(26) Egorova, D.; Domcke, W. *J. Photochem. Photobiol. A Chem.* **2004**, *166*, 19–31.

(27) Lin, S. W.; Groesbeek, M.; van der Hoef, I.; Verdegem, P.; Lugtenburg, J.; Mathies, R. *J. Phys. Chem. B* **1998**, *102*, 2787–806.

(28) Kukura, P.; McCamant, D. W.; Yoon, S.; Wandschneider, D. B.; Mathies, R. *Science* **2005**, *310*, 1006–9.

(29) Pollard, W. T.; Dexheimer, S. L.; Wang, Q.; Peteanu, L. A.; Shank, C. V.; Mathies, R. *J. Phys. Chem.* **1992**, *96*, 6147–58.

(30) Dexheimer, S. L.; Wang, Q.; Peteanu, L. A.; Pollard, W. T.; Mathies, R.; Shank, C. V. *Chem. Phys. Lett.* **1992**, *188*, 61–6.

(31) Ruhman, S.; Kohler, B.; Joly, A. G.; Nelson, K. A. *IEEE J. Quantum Electron.* **1988**, *24*, 470–81.

(32) Ruhman, S.; Joly, A. G.; Nelson, K. A. *IEEE J. Quantum Electron.* **1988**, *24*, 460–9.

(33) Weingart, O.; Altoè, P.; Stenta, M.; Bottoni, A.; Orlandi, G.; Garavelli, M. *Phys. Chem. Chem. Phys.* **2011**, *13*, 3645–8.

(34) Gozem, S.; Melaccio, F.; Lindh, R.; Krylov, A. I.; Granovsky, A. A.; Angeli, C.; Olivucci, M. *J. Chem. Theory Comput.* **2013**, *9*, 4495–4506.

(35) Loppnow, G. R.; Mathies, R. A. *Biophys. J* **1988**, *54*, 35–43.

(36) De Grip, W. J.; Daemen, F. J.; Bonting, S. L. *Methods Enzymol.* **1980**, *67*, 301–20.

(37) Trebino, R.; DeLong, K. W.; Fittinghoff, D. N.; Sweetser, J. N.; Krumbugel, M. A.; Richman, B. A.; Kane, D. J. *Rev. Sci. Instrum.* **1997**, *68*, 3277–95.

For Table of Contents Only